A massive rock and ice avalanche caused the 2021 disaster at Chamoli, Indian Himalaya

Shugar, D. H.; Jacquemart, M.; Shean, D.; Bhushan, S.; Upadhyay, K.; Sattar, A.

Published in:
Science (New York, N.Y.)

DOI:
10.1126/science.abh4455

Publication date:
2021

Document Version
Peer reviewed version

A massive rock and ice avalanche caused the 2021 disaster at Chamoli, Indian Himalaya

Authors: Shugar, D.H.[1*], Jacquemart, M.[2,3,4], Shean, D.[5], Bhushan, S.[5], Upadhyay, K.[6], Sattar, A.[7], Schwanghart, W.[8], McBride, S.[9], Van Wyk de Vries, M.[10,11], Mergili, M.[12,13], Emmer, A.[12], Deschamps-Berger, C.[14], McDonnell, M.[15], Bhambri, R.[16], Allen, S.[7,17], Berthier, E.[18], Carrivick, J.L.[19], Clague, J.J.[20], Dokukin, M.[21], Dunning, S.A.[22], Frey, H.[7], Gascoin, S.[14], Haritashya, U.K.[23], Huggel, C.[7], Kääb, A.[24], Kargel, J.S.[25], Kavanaugh, J.L.[26], Lacroix, P.[27], Petley, D.[28], Rupper, S.[15], Azam, M.F.[29], Cook, S.J.[30,31], Dimri, A.P.[32], Eriksson, M.[33], Farinotti, D.[3,4], Fiddes, J.[34], Gnyawali, K.R.[35], Harrison, S.[36], Jha, M.[37], Koppes, M.[38], Kumar, A.[39], Leinss, S.[40,41], Majeed, U.[42], Mal, S.[43], Muhuri, A.[14,44], Noetzli, J.[34], Paul, F.[7], Rashid, I.[42], Sain, K.[39], Steiner, J.[45,46], Ugalde, F.[47,48], Watson, C.S.[49], Westoby, M.J.[50]

Affiliations:

[1]Water, Sediment, Hazards, and Earth-surface Dynamics (waterSHED) Lab, Department of Geoscience; University of Calgary, AB, Canada.
[2]Cooperative Institute for Research in Environmental Sciences, University of Colorado; Boulder, CO, USA.
[3]Laboratory of Hydraulics, Hydrology and Glaciology (VAW), ETH Zurich; Zurich, Switzerland.
[4]Swiss Federal Institute for Forest, Snow and Landscape Research WSL; Birmensdorf, Switzerland.
[5]Department of Civil and Environmental Engineering, University of Washington; Seattle, WA, USA.
[6]Independent journalist/water policy researcher; Nainital, Uttarakhand, India.
[7]Department of Geography, University of Zurich; Zurich, Switzerland.
[8]Institute of Environmental Science and Geography, University of Potsdam; Potsdam, Germany.
[9] U.S. Geological Survey, Earthquake Science Center; Moffett Field, CA, USA.
[10]Department of Earth & Environmental Sciences, University of Minnesota, Minneapolis, MN, USA.
[11]St. Anthony Falls Laboratory, University of Minnesota; Minneapolis, MN, USA.
[12]Institute of Geography and Regional Science, University of Graz; Graz, Austria.
[13]Institute of Applied Geology, University of Natural Resources and Life Sciences (BOKU); Vienna, Austria.
[14]CESBIO, Université de Toulouse, CNES/CNRS/INRAE/IRD/UP; Toulouse, France.
[15]Department of Geography, University of Utah; Salt Lake City, Utah, USA.
[16]Department of Geography, South Asia Institute, Heidelberg University; Heidelberg, Germany.
[17]Institute for Environmental Sciences, University of Geneva; Switzerland.
[18]LEGOS, Université de Toulouse, CNES/CNRS/IRD/UPS; Toulouse, France.
[19]School of Geography and water@leeds, University of Leeds, Leeds; West Yorkshire, UK.
[20]Department of Earth Sciences, Simon Fraser University; Burnaby, BC, Canada.
[21]Department of Natural Disasters, High-Mountain Geophysical Institute; Nalchik, Russia.
[22]Geography, Politics and Sociology, Newcastle University; Newcastle, UK.

DOI: 10.1126/science.abh4455.

[23]Department of Geology and Environmental Geosciences, University of Dayton; Dayton, OH, USA.
[24]Department of Geosciences, University of Oslo; Oslo, Norway.
[25]Planetary Science Institute; Tucson, AZ, USA.
[26]Earth and Atmospheric Sciences, University of Alberta; Edmonton, AB, Canada.
[27]ISTerre, Université Grenoble Alpes, IRD, CNRS; Grenoble, France.
[28]Department of Geography, The University of Sheffield; Sheffield, UK.
[29]Indian Institute of Technology Indore; India.
[30]Geography and Environmental Science, University of Dundee; Dundee, UK.
[31]UNESCO Centre for Water Law, Policy and Science, University of Dundee; Dundee, UK.
[32]School of Environmental Sciences, Jawaharlal Nehru University; New Delhi, India.
[33]Stockholm International Water Institute; Stockholm, Sweden.
[34]WSL Institute for Snow and Avalanche Research SLF; Davos, Switzerland.
[35]School of Engineering, University of British Columbia; Kelowna, BC, Canada.
[36]College of Life and Environmental Sciences, University of Exeter, Penryn, UK.
[37]Department of Mines and Geology, National Earthquake Monitoring and Research Center; Kathmandu, Nepal.
[38]Department of Geography, University of British Columbia; Vancouver, BC, Canada.
[39]Wadia Institute of Himalayan Geology, Dehradun; Uttarakhand, India.
[40]Institute of Environmental Engineering (IfU), ETH Zurich, 8093 Zürich, Switzerland
[41]Current affiliation: LISTIC, Université Savoie Mont Blanc, 74940 Annecy, France
[42]Department of Geoinformatics, University of Kashmir; Hazratbal Srinagar, Jammu and Kashmir, India.
[43]Department of Geography, Shaheed Bhagat Singh College, University of Delhi; Delhi, India.
[44]Institute of Geography, Heidelberg University; Germany.
[45]International Centre for Integrated Mountain Development; Kathmandu, Nepal.
[46]Department of Physical Geography, Utrecht University; Netherlands.
[47]Geoestudios, San José de Maipo; Chile.
[48]Department of Geology, University of Chile; Santiago, Chile.
[49]COMET, School of Earth and Environment. University of Leeds; Leeds, UK.
[50]Department of Geography and Environmental Sciences, Northumbria University; Newcastle upon Tyne, UK.

*Corresponding author. Email: daniel.shugar@ucalgary.ca

Abstract: On 7 Feb 2021, a catastrophic mass flow descended the Ronti Gad, Rishiganga, and Dhauliganga valleys in Chamoli, Uttarakhand, India, causing widespread devastation and severely damaging two hydropower projects. Over 200 people were killed or are missing. Our analysis of satellite imagery, seismic records, numerical model results, and eyewitness videos reveals that ~27×10^6 m^3 of rock and glacier ice collapsed from the steep north face of Ronti Peak. The rock and ice avalanche rapidly transformed into an extraordinarily large and mobile debris flow that transported boulders >20 m in diameter, and scoured the valley walls up to 220 m above the valley floor. The intersection of the hazard cascade with downvalley infrastructure resulted in a disaster, which highlights key questions about adequate monitoring and sustainable development in the Himalaya as well as other remote, high-mountain environments.

One-Sentence Summary: The Chamoli disaster was triggered by an extraordinary rock and ice avalanche and debris flow, that destroyed infrastructure and left 204 people dead or missing.

Main Text: Steep slopes, high topographic relief, and seismic activity make mountain regions prone to extremely destructive mass movements (e.g. *1*). The sensitivity of glaciers and permafrost to climate changes is exacerbating these hazards (e.g. *2–7*). Hazard cascades, where an initial event causes a downstream chain reaction (e.g. *8*), can be particularly far-reaching, especially when they involve large amounts of water (*7*, *9*, *10*). An example is the 1970 Huascarán avalanche, Peru, that was one of the largest, farthest-reaching, and deadliest (~6000 lives lost) mass flows (*11*). Similarly, in 2013, over 4,000 people died at Kedarnath, Uttarakhand, India, when a moraine-dammed lake breached following heavy rainfall and snowmelt (*12–14*). Between 1894 and 2021, the Uttarakhand Himalaya has witnessed at least 16 major disasters from flash floods, landslides, and earthquakes (*14*, *15*).

Human activities that intersect with the mountain cryosphere can increase risk (*16*) and are common in Himalayan valleys where hydropower development is proliferating due to growing energy demands, the need for economic development, and efforts to transition into a low-carbon society (*17*, *18*). Hydropower projects in Uttarakhand and elsewhere in the region have been opposed over their environmental effects, public safety, and issues associated with justice and rehabilitation (*19*, *20*).

On 7 Feb 2021, a massive rock and ice avalanche from the 6063 m-high Ronti Peak generated a cascade of events that caused more than 200 deaths or missing persons, as well as damage or destruction of infrastructure that most notably included two hydropower projects in the Rishiganga and Dhauliganga valleys (Fig. 1, table S1) (*21*). Here, we present a rapid and comprehensive reconstruction of the hazard cascade. We leveraged multiple types of remote sensing data, eyewitness videos, numerical modeling, seismic data, and reconnaissance field observations in a collaborative, global effort to understand this event. We also describe the antecedent conditions and the immediate societal response, allowing us to consider some wider implications for sustainable development in high-mountain environments.

February 7 2021 hazard cascade

At 4:51 UTC (10:21 Indian Standard Time [IST]), about 26.9×10^6 m^3 (95% confidence interval: 26.5-27.3×10^6 m^3) of rock and ice (Fig. 1, 2) detached from the steep north face of Ronti Peak at an elevation of about 5,500 m asl, and impacted the Ronti Gad (‘gad’ means rivulet) valley floor

about 1,800 m below. We estimated the onset of this avalanche and its velocity by analyzing seismic data from two distant stations, 160 and 174 km southeast of the source (Fig. S6) (*22*, §5.1). The initial failure happened between 4:51:13 and 4:51:21 UTC, based on a source-sensor wave travel-time correction. We attributed a high-frequency signal 55 to 58 seconds later to the impact of the avalanche on the valley bottom, indicating a mean speed of the rock and ice avalanche of between 57 and 60 ms^{-1} (205 to 216 km h^{-1}) down the ~35° steep mountain face.

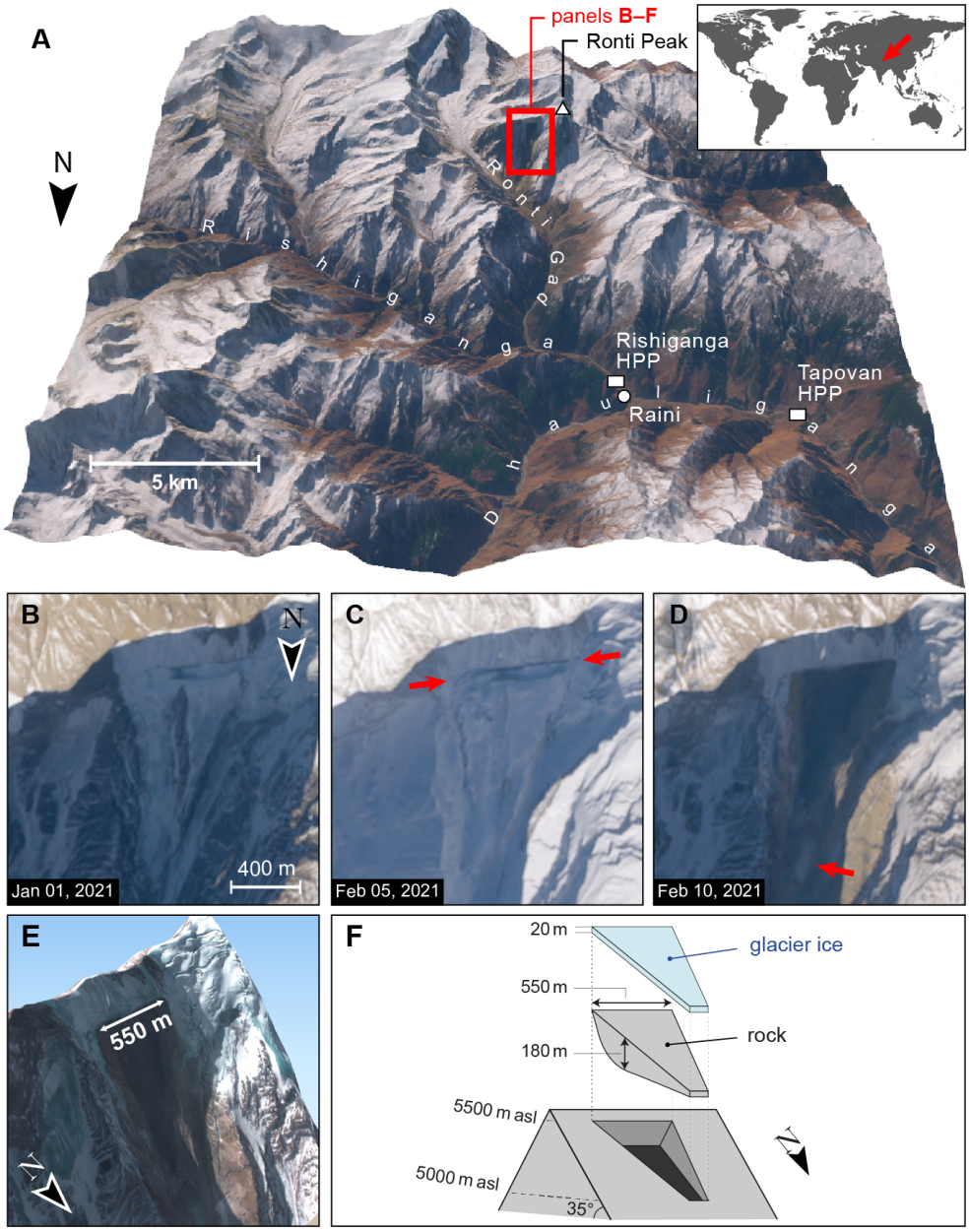

Fig. 1. Overview of the Chamoli disaster, Uttarakhand, India. (**A**) 3D rendering of the local geography, with labels for main place names mentioned in the text. HPP stands for hydropower project. (**B-D**) Pre- and post-event satellite imagery of the site of the collapsed rock and glacier block, and the resulting scar. Note snow cover in the region just before the event (C). The red arrows in (C) mark the fracture that became the headscarp of the landslide (*22*, §3.2 and fig. S4).

The arrow in D points to a remaining part of the lower eastern glacier. (**E**) 3D rendering of the scar. (**F**) Schematic of failed mass of rock and ice. Satellite imagery in (A–D) and (E) is from Sentinel-2 (Copernicus Sentinel Data 02-10-2021) and Pléiades-HR (© CNES 02-10-2021, Distribution AIRBUS DS), respectively.

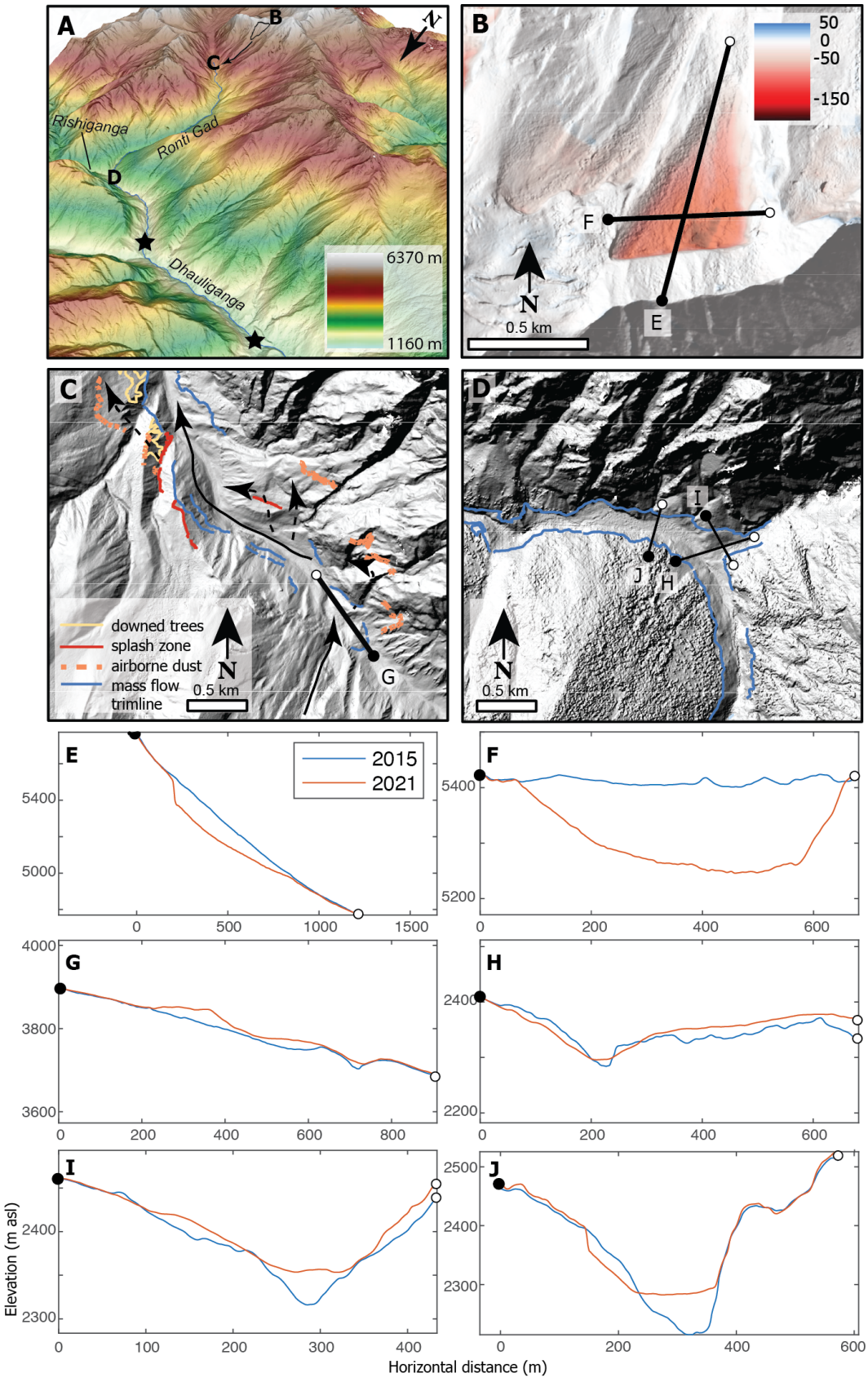
A
B
C
D
Rishiganga
Ronti Gad
Dhauliganga
6370 m
1160 m
N
B
50
0
-50
-150
F
E
N
0.5 km
C
downed trees
splash zone
airborne dust
mass flow
trimline
N
0.5 km
G
D
I
J
H
N
0.5 km
E
2015
2021
5400
5000
0
500
1000
1500
F
5400
5200
0
200
400
600
G
4000
3800
3600
0
200
400
600
800
H
2400
2200
0
200
400
600
I
2400
2300
0
100
200
300
400
J
2500
2400
2300
0
200
400
600
Elevation (m asl)
Horizontal distance (m)

142

Fig. 2. Satellite-derived elevation data of the Chamoli hazard cascade. (A) Perspective view of the area, from the landslide source at Ronti Peak to the Rishiganga and Tapovan Vishnugad hydropower projects (black stars). (**B)** Elevation change over the landslide scar based on DEM-differencing between September 2015 and February 10-11, 2021. (**C**) The proximal valley floor, with geomorphic interpretations of the flow path. (**D)** Confluence of Ronti Gad and Rishiganga River. (**E-J)** Topographic profiles showing elevation change due to rock/icefall and sediment deposition for locations shown in (**B-D**). Elevation loss on the inner bank in (J) is primarily due to the destruction of forest.

Differencing of high-resolution digital elevation models (DEMs) revealed a failure scar that has a vertical difference of up to 180 m and a slope-normal thickness of ~80 m on average, and a slab width up to ~550 m, including both bedrock and overlying glacier ice (Fig. 2). The lowermost part of the larger eastern glacier is still in place and was not eroded by the rock and ice avalanche moving over it (Fig. 1D), suggesting that the avalanche may have become airborne for a short period during its initial descent. Optical feature tracking detected movement of the failed rock block as early as 2016, with the largest displacement in the summer months of 2017 and 2018 (fig. S4). This movement opened a fracture up to 80 m wide in the glacier and into the underlying bedrock (Fig. 1, fig. S5). Geodetic analysis and glacier thickness inversions indicate that the collapsed mass comprised ~80% rock and ~20% glacier ice by volume (*22*, §5.2, fig. S10). Melt of this ice was essential to the downstream evolution of the flow, as water transformed the rock and ice avalanche into a highly mobile debris flow (cf. *23*, *24*). Media reports (*25*) suggest that some ice blocks (diameter <1 m) were found in tunnels at the Tapovan Vishnugad hydropower site (hereafter referred to as the Tapovan project), and some videos of the debris flow (*22*, §5.3) show floating blocks that we interpret as ice, indicating that some of the ice survived at considerable distance downstream. Notably, and in contrast to most previously documented rock avalanches, very little debris is preserved at the base of the failed slope. This is likely due to the large volumes of water (*22*, §5.5) that resulted in a high mobility of the flow.

Geomorphic mapping based on very high-resolution satellite images (Table S2) acquired during and immediately after the event, provides evidence of the flow evolution. We detected four components of the catastrophic mass flow, beginning with the main rock and ice avalanche from Ronti Peak described above (component one).

The second component is “splash deposits” (cf. *26–28*), which are relatively fine-grained, wet sediments that became airborne as the mass flow ran up adjacent slopes. For example, the rock and ice avalanche traveled up a steep slope on the east side of the valley opposite the source zone, and some material became airborne, being deposited at a height of about 120 m above the valley floor. These deposits include boulders up to ~8 m (a-axis length). The bulk of the flow then traveled back to the proximal (west) side of the valley and rode up a ridge ~220 m above the valley floor, before becoming airborne and splashing into a smaller valley to the west (Fig. 2C, figs. S15, S18). Boulders up to 13 m (a-axis length) were deposited near the top of the ridge. Vegetation remained intact on the lee side of some ridges that were overrun by the splashing mass.

A third component of the mass flow is reflected in airborne dust deposition. A dust cloud is visible in PlanetScope imagery from 5:01 UTC and 5:28 UTC February 7 (10:31 and 10:58 IST). A smooth layer of debris, estimated from satellite imagery to be only a few cm in thickness, was deposited higher than the splash deposits, up to ~500 m above the valley floor, although the boundary between the airborne dust deposition and other mass flow deposits is indistinct in places. Signs of the largely airborne splash and dust components can be observed over ~3.5 km downstream of the valley impact site. The avalanche also generated a powerful air blast (cf. *1*) that flattened about 0.2 km^2 of forest on the west side of the Ronti Gad valley (Fig. 2C).

After the rock and ice avalanche impacted the valley floor, most of it moved downvalley in a northwesterly direction. Frictional heating of the ice in the avalanche generated liquid water that allowed the transition in flow characteristics, becoming more fluid downvalley, creating a flow consisting of sediment, water, and blocks of ice. The uppermost part of the valley floor deposits is around 0.75 $x10^6$ m^3, with remarkably few large boulders that typically form the upper surface of rock avalanches (e.g. *29*, *30*) (Fig. 2G, fig. S16). The mass flow traveled downvalley and superelevated (runup elevation) up to ~130 m above the valley floor around bends (fig. S17). Clear trimlines, at some places at multiple levels, are evident along much of the flow path (e.g. Fig. 2C, D).

At the confluence of the Ronti Gad and Rishiganga River, a ~40 m thick deposit of debris blocked the Rishiganga valley (Fig. 2H, I). Deposition in this area probably resulted from deceleration of the mass flow at a sharp turn to the west. During the days following the event, a lake ~700 m long formed behind these deposits in the Rishiganga valley upstream of its confluence with Ronti Gad. The lake was still present two months later and had grown since the initial formation. Substantial deposition occurred about 1 km downstream of the confluence, where material up to ~100 m thick was deposited on the valley floor (Fig. 2J). DEM differencing shows that the total deposit volume at the Ronti Gad-Rishiganga River confluence and just downstream was ~$8x10^6$ m^3. These large sediment deposits likely indicate the location where the flow transitioned to a debris flow (*31*) - the fourth component.

A field reconnaissance by co-authors from the Wadia Institute of Himalayan Geology indicates that the impact of debris flow material (sediment, water, ice, woody debris) at the confluence of Rishiganga River with Dhauliganga River created a bottleneck and forced some material 150-200 m up the Dhauliganga (fig. S15). The release of the water a few minutes later led to the destruction of a temple on the north bank of the Dhauliganga.

A substantial fraction of the fine-grained material involved in the event was transported far downstream. This more dilute flow could be considered a fifth component. Approximately 24 hours after the initial landslide, the sediment plume was visible in PlanetScope and Sentinel-2 imagery in the hydropower project's reservoir on the Alaknanda River at Srinagar, about 150 km downstream from the source. About 2½ weeks later, increased turbidity was observed at Kanpur on the Ganges River, ~900 km from the source. An official of the Delhi water quality board reported that 8 days after the Chamoli disaster, a chief water source for the city - a canal drawing directly from the Ganga River - had an unprecedented spike in suspended sediment (turbidity) 80 times the permissible level (*32*). The amount of corresponding sedimentation in

hydropower reservoirs and rivers is unknown, but possibly substantial, and may contribute to increased erosion on turbine blades, and infilling of reservoirs in the years to come.

Analysis of eyewitness videos permitted estimation of the propagation of the flow front below the Ronti Gad-Rishiganga River confluence (Fig. 3, *22*, §5.3). The maximum frontal velocity reconstructed from these videos is ~25 m s^{-1} near the Rishiganga hydropower project (fig. S11, table S5), which is about 15 km downstream of the rock and ice avalanche source. Just upstream of the Tapovan project (another ~10 km downriver), the velocity decreased to ~16 m s^{-1}, and just downstream of Tapovan (26 km from source), the velocity was ~12 m s^{-1}. The large reduction in frontal velocity is likely related to impoundment behind the Tapovan project dam. Analysis of PlanetScope images (at 5:01 UTC and 5:28 UTC) suggests that the average frontal velocity between Raini (at Rishiganga hydropower project) and Joshimath (16 km downstream) was ~10 m s^{-1}. We also estimated mean discharge from the videos to be between ~8,200 and ~14,200 m^3 s^{-1} at the Rishiganga hydropower project and between ~2,900 and ~4,900 m^3 s^{-1} downstream of the Tapovan project. Estimates for the debris flow duration are complicated by uncertain volumes, water contents, discharge amounts, and shapes of discharge curves at specific locations. For Rishiganga, for example, we estimate a duration of 10-20 minutes, a number that appears realistic from the information available.

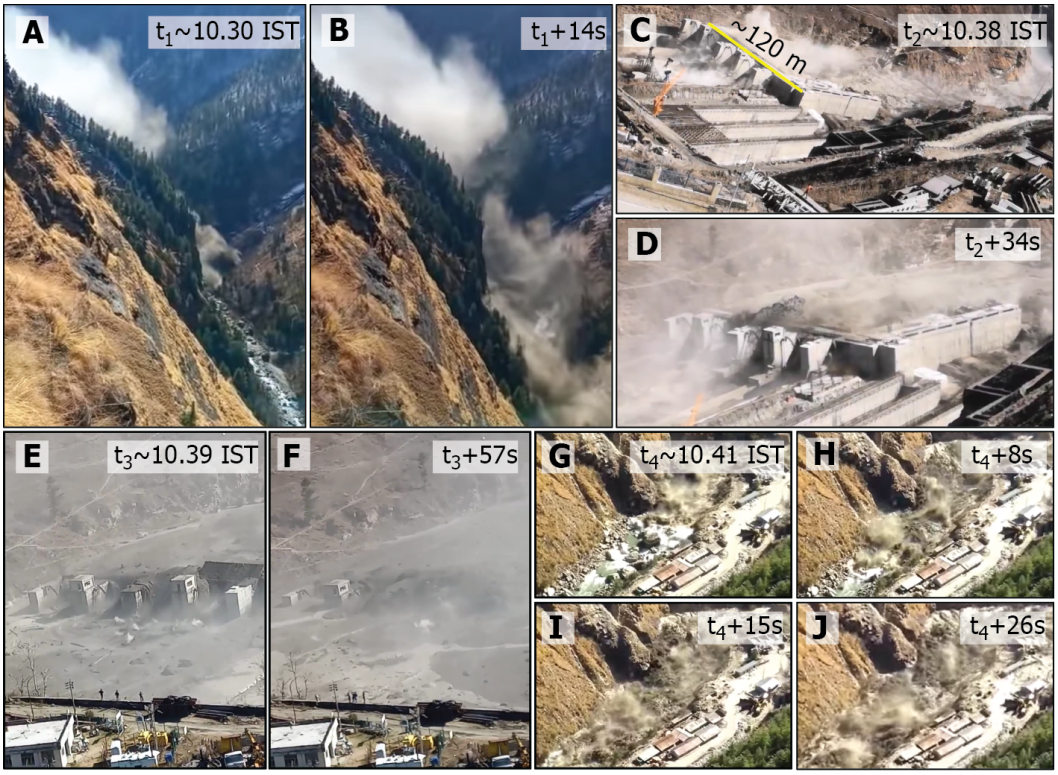

Parts a-b: Electricity Market in India: Dhauliganga 4*70 MW Coffer Dam collapse in Uttarakhand Chamoli... Prayers for Uttarakhand; URL: https://www.youtube.com/watch?v=96nopxNn-Qp4&t=1s; accessed: 28th February 2021
Parts c-d: Kamlesh Maikhuri (https://www.facebook.com/100005762340793/videos/1678161685719227/ (since removed)) ; Permission: verbal permission of the author given to Kavita Upadhyay
Parts e-f: Manvar Rawat (https://www.facebook.com/100007108448247/videos/2796749477238640/) ; Permission: verbal permission of the author given to Kavita Upadhyay
Parts g-j: RW • Rishikeshwritings: Uttarakhand Flood 2021|| Rishikesh , Srinagar , Devprayag , Haridwar; URL: https://www.youtube.com/watch?v=QE0iPLq8gbY; accessed: 28th February

Fig. 3. Sample video frames used to analyse flood velocity and discharge. (**A,B**) Flow front arrives and rushes through the valley upstream of the Rishiganga project (location P1 in Fig. 4). (**C**) Flow front arrives at Tapovan project's dam (location P3). (**D**) The reservoir is being filled quickly; spillways are damaged. (**E**) The dam is overtopped. (**F**) Collapse of

remaining structures. (**G-J**) Flow front proceeds down the valley below the Tapovan dam (location P4); spreading into the village in (J).

We conducted numerical simulations with r.avaflow (*22*, §5.4), which indicate that the rock and ice avalanche could not have transitioned to the debris flow seen farther downstream without an accompanying reduction in the debris volume. If such a direct transition had occurred, the modeling suggests that the flow discharge would be approximately one order of magnitude higher than the estimates derived from video recordings (*22*, §5.4). The deposition patterns we observed in satellite imagery support the hypothesis that the vicinity of the Ronti Gad-Rishiganga River confluence played a key role in flow transition. Our numerical simulations are consistent with the escape of a fluid-rich front from the rock and ice avalanche mass near this confluence (Fig. 4A), reproducing mapped trimlines and estimated flow velocities and discharges down to Tapovan (Fig. 4B, C). Our simulated discharge estimates at P1–P4 are within the ranges derived from the video analysis (Fig. 4D, *22*, §5.3), and simulated travel times between P0-P3 (Fig. 4D) show excellent agreement (<5% difference) with travel times inferred from seismic data, videos, and satellite imagery. We found less agreement between the numerical model results and the reconstructions from videos farther downstream due to the complex effects of the Tapovan project in slowing the flow, which are at a finer scale than is represented by our model.

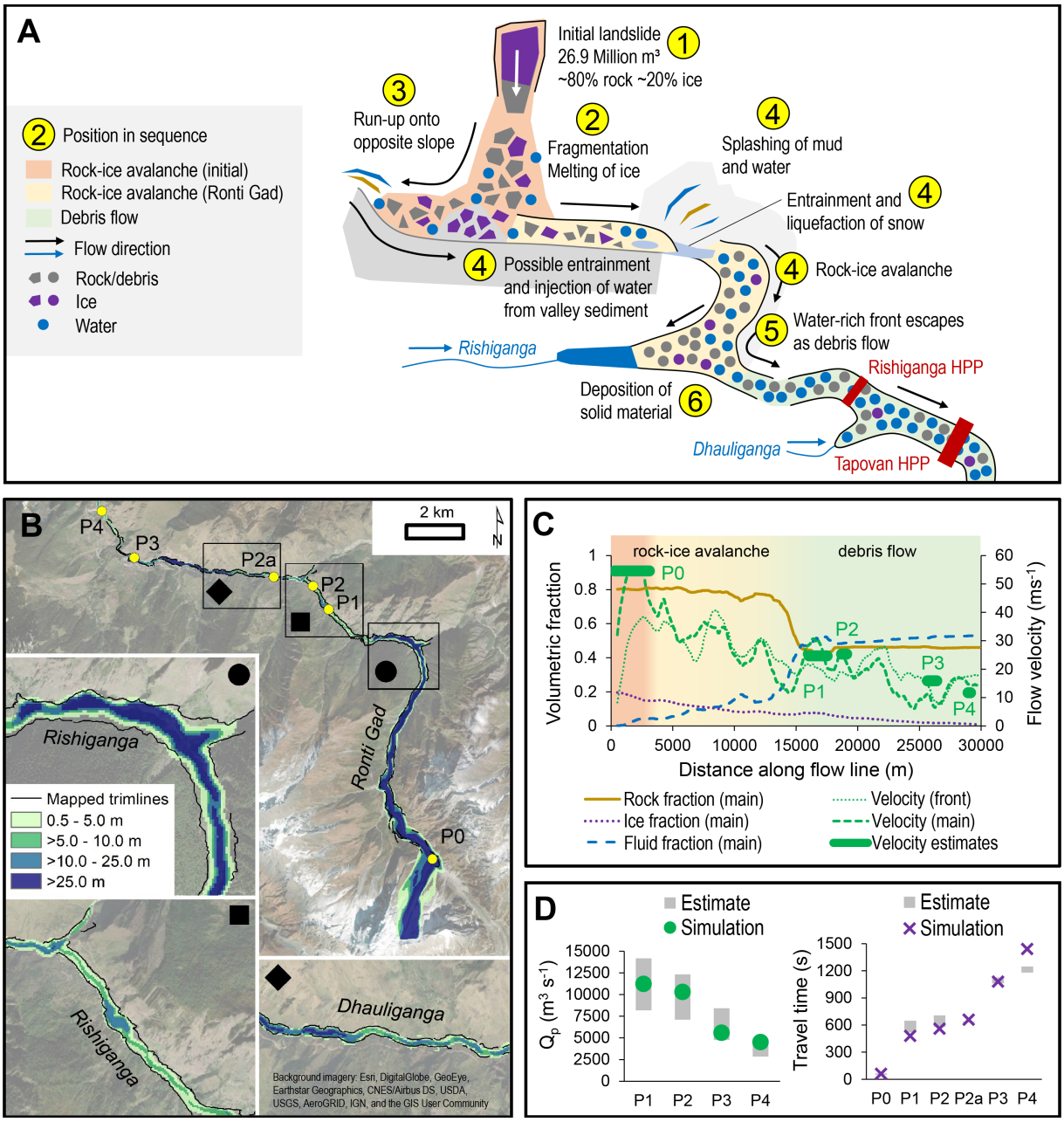

Fig. 4. Flow evolution scenarios and simulation. (**A**) Schematic of the evolution of the flow from the source to Tapovan. (**B**) Maximum flow height simulated with r.avaflow, showing the observed trim lines for comparison. P0 is the location of the velocity estimate derived from seismic data, P1-P4 are locations of velocity estimates based on videos and satellite images. (**C**) Along-profile evolution of flow velocity and fractions of rock/debris, ice, and water simulated with r.avaflow. (**D**) Simulated and estimated peak discharges and travel times at above locations. In the legend labels, (front) refers to the flow front whereas (main) refers to the point of maximum flow momentum.

Causes and implications

The February 7 rock and ice avalanche was a very large event with an extraordinarily high fall height that resulted in a disaster due to its extreme mobility and the presence of downstream infrastructure. The ~3700 m vertical drop to the Tapovan HPP is surpassed clearly by only two known events in the historic record, namely the 1962 and 1970 Huascaran avalanches (*11*), while its mobility (H/L = 0.16 at Tapovan, where H is fall height and L is flow length) is exceeded only by a few recent glacier detachments (*10*). The location of the failure was due to the extremely steep and high relief of Ronti Peak. The sheared nature of the source rocks and contrasting interbedded rock types likely conditioned the failure (*22*, §1). The large and expanding fracture (Fig 1B, C) at the head scarp may have allowed liquid water to penetrate into the bedrock, increasing pore-water pressures or enhancing freeze-thaw weathering.

Nearly all (190) of the 204 people either killed or missing in the disaster (*22*, §2, Table S1) were workers at the Rishiganga (13.2 MW) and Tapovan (520 MW) project sites (*33*). Direct economic losses from damage to the two hydropower structures alone are over 223 million USD (*34*, *35*). The high loss of human life and infrastructure damage was due to the debris flow, and not the initial rock and ice avalanche. However, not all large, high-mountain rock and ice avalanches transform into highly mobile debris flows that cause destruction far from their source (*9*).

Our energy balance estimates indicate that most of the ~5-6x10^6 m^3 volume of glacier ice first warmed (along with a portion of the rock mass) from approximately -8ºC to 0ºC and then melted through frictional heating during the avalanche as it descended to the Rishiganga valley, involving a drop of approximately 3400 m (*22*, §5.5). Potential other sources of water were considered, including glacier lake outburst floods, catastrophic drainage of water from reservoirs such as surface lakes, ice deposited by earlier avalanches, and enlithic reservoirs. No evidence for such sources was observed in available remote sensing data. A slow-moving storm system moved through the area in the days before Feb 7. We estimate that a ~220,000–360,000 m^3 contribution from precipitation over the Ronti Gad basin was a minor component of the flow, representing only 4-7% of the water equivalent contained in the initial glacier ice detachment. Similarly, while water already present in the river, water ejected from groundwater, melting snow, wet sediment, and water released from the run-of-the-river hydroelectric project may have all contributed to the debris flow, even when taken together (with generous error margins), these sum to a small amount compared to the probable range of water volumes in the mass movement. The major effect of ice melt on the mobility of rock and ice avalanches is documented (*9*, *10*), but it appears that the combination of the specific rock/ice fraction (~80/20% by volume) and large fall height of the rock and ice avalanche led to a rare, severe event during which nearly all of the ice melted.

Soon after the disaster, media reports and expert opinions started to circulate, postulating links of the event to climate change. Recent attribution studies demonstrated that glacier mass loss on global, regional and local scales is to a large extent attributable to anthropogenic greenhouse gas forcing (*36*, *37*). High-mountain slope failures in rock and ice, however, pose additional challenges to attribution due to multiple factors and processes involved in such events. While long-term trends of increasing slope failure occurrence in some regions

could be attributed to climate change (*16*, *38*, *39*), attribution of single events such as the Chamoli event remains largely elusive. Nevertheless, certain elements of the Chamoli event have potential links to climate, and weather, as described below. Furthermore, the Chamoli event may be seen in the context of a change in geomorphological sensitivity (*40*) and might therefore be seen as a precursor for an increase in such events as climate warming proceeds.

The stability of glacierized and perennially frozen high-mountain slopes is indeed particularly sensitive to climate change (*16*). Our analysis suggests regional climate and related cryospheric change could have interacted in a complex way with the geologic and topographic setting to produce this massive slope failure. Air and surface temperatures have been increasing across the Himalayan region, with greater rates of warming during the second half of the 20th Century and at higher elevations (*41*, *42*). Most glaciers in the Himalaya are shrinking and mass loss rates are accelerating across the region (*22*, §1, *43–46*). Glacier shrinkage uncovers and destabilizes mountain flanks and strongly alters the hydrological and thermal regimes of the underlying rock.

The detachment zone at Ronti Peak is about 1 km higher than the regional lower limit of permafrost at around 4,000 to 4,500 m asl., as indicated by rock glaciers in the region and global permafrost maps (*47*, *48*). Exposed rock on the north face of Ronti Peak likely contains cold permafrost with rock temperatures several degrees below 0°C. In connection with glaciers, however, ground temperatures can be locally higher. The ice-free south face of Ronti Peak is certainly substantially warmer with rock temperatures perhaps around or above 0°C, causing strong south-to-north lateral heat fluxes (*49*). Permafrost temperatures are increasing worldwide, in particular in cold permafrost (*16*, *50*, *51*), leading to long-term and deep-seated thermal anomalies, and even permafrost degradation (*49*). Increasing ground temperatures at the failure site of the Chamoli avalanche could have resulted in reduced strength of the frozen rock mass by altering the rock hydrology and the mechanical properties of discontinuities and the failed rock mass (*52*).

The geology of the failed rocks includes several observed or inferred critical attributes (*22*, §1): (i) The rocks are cut by multiple directions of planar weaknesses; the failed mass detached along four of these. (ii) The rock mass is close to a major thrust fault, with many local shear fractures, which - along with other discontinuities - would have facilitated aqueous chemical weathering. (iii) The rock types (schist and gneiss), even when nominally unweathered, contain abundant soft, platy, oriented, and geomechanically anisotropic minerals (phyllosilicates and kyanite especially); Weathering will further weaken these rocks, and they will be more likely to disintegrate into fine material upon impact, which would influence the rheology and likely enhance the mobility of the mass flow.

Importantly, the 7 Feb failure considerably changed the stress regime and thermal conditions in the area of the detachment zone. Only detailed investigations and monitoring will determine whether rock or ice adjacent to the failed block (including a large hanging rock block above the scarp) were destabilized due to these changes and present an ongoing hazard. Similarly, the impoundment at the Ronti Gad-Rishiganga River confluence requires careful monitoring as embedded ice in the dam deposits may melt with warmer temperatures,

increasing the risk of an outburst flood by reducing lake freeboard of the dam, and/or reducing structural coherence of the dam.

Videos of the event, including the ones broadcast on social media in real time (*22*, §5.3), showed that the people directly at risk had little to no warning. This leads us to question what could have happened if a warning system had been installed. We estimate that a suitably designed early warning system might have allowed for 6 to 10 minutes of warning before the arrival of the debris flow at the Tapovan project (perhaps up to 20 minutes if situated near the landslide source, or if a dense seismic network was leveraged (*53*)), which may have provided enough time to evacuate at least some workers from the power project. After the event, a new flood warning system was installed near Raini (*22*, §2.1, fig. S15D). Studies show that early warning system design and installation is technically feasible but rapid communication of reliable warnings and appropriate responses by individuals to alerts, are complex (*54*). Previous research indicates that effective early warning requires public education, including drills, which would increase awareness of potential hazards and improve ability to take action when disaster strikes (*55*, *56*). Considering the repeated failures from the same slope in the past two decades (*22*, §1), public education and drills in the Chamoli region would be very beneficial.

Conclusions

On the morning of 7 Feb 2021, a large rock and ice avalanche descended the Ronti Gad valley, rapidly transforming into a highly mobile debris flow that destroyed two hydropower plants and left more than 200 people dead or missing. We identified three primary drivers for the severity of the Chamoli disaster: (1) the extraordinary fall height, providing ample gravitational potential energy; (2) the worst-case rock:ice ratio, which resulted in almost complete melting of the glacier ice, enhancing the mobility of the debris flow; and (3) the unfortunate location of multiple hydropower plants in the direct path of the flow.

The debris flow disaster started as a wedge failure sourced in bedrock near the crest of Ronti Peak, and included an overlying hanging glacier. The rock almost completely disintegrated in the ~1 minute that the wedge took to fall (~5500 – 3,700 m asl), and the rock:ice ratio of the detached mass was almost exactly the critical value required for near-complete melting of the ice. As well as having a previous history of large mass movements, the mountain is riven with planes and points of structural weakness, and further bedrock failures as well as large ice and snow avalanches are inevitable.

Videos of the disaster were rapidly distributed through social media, attracting widespread international media coverage and catalyzing an immediate response from the international scientific community. This response effort quickly leveraged images from modern commercial and civilian government satellite constellations that offer exceptional resolution, "always-on" cadence, rapid tasking, and global coverage. This event demonstrated that if appropriate human resources and technologies are in place, post-disaster analysis can be reduced to days or hours. Nevertheless, ground-based evidence remains crucial for clarifying the nature of such disasters.

Although we cannot attribute this individual disaster specifically to climate change, the possibly increasing frequency of high-mountain slope instabilities can likely be related to observed atmospheric warming and corresponding long-term changes in cryospheric conditions (glaciers, permafrost). Multiple factors beyond those listed above contributed to the Chamoli rock and ice avalanche, including the geologic structure and steep topography, possible long-term thermal disturbances in permafrost bedrock induced by atmospheric warming, stress changes due to the decline and collapse of adjacent and overlying glaciers, and enhanced melt water infiltration during warm periods.

The Chamoli event also raises important questions about clean energy development, climate change adaptation, disaster governance, conservation, environmental justice, and sustainable development in the Himalaya and other high-mountain environments. This stresses the importance of a better understanding of the cause and impact of mountain hazards, leading to disasters. While the scientific aspects of this event are the focus of our study, we cannot ignore the human suffering and emerging socio-economic impacts that it caused. It was the human tragedy that motivated the authors to examine available data and explore how these data, analyses, and interpretations can be used to help inform decision-making at the ground level.

The disaster tragically revealed the risks associated with the rapid expansion of hydropower infrastructure into increasingly unstable territory. Enhancing inclusive dialogues among governments, local stakeholders and communities, private sector, and the scientific community could help assess, minimize, and prepare for existing risks. The disaster indicates that the long-term sustainability of planned hydroelectric power projects must account for both current and future social and environmental conditions, while mitigating risks to infrastructure, personnel, and downstream communities. Conservation values carry elevated weight in development policies and infrastructure investments where the needs for social and economic development interfere with areas prone to natural hazards, putting communities at risk.

References

1. J. S. Kargel, G. J. Leonard, D. H. Shugar, U. K. Haritashya, A. Bevington, E. J. Fielding, K. Fujita, M. Geertsema, E. S. Miles, J. Steiner, E. Anderson, S. Bajracharya, G. W. Bawden, D. F. Breashears, A. Byers, B. Collins, M. R. Dhital, A. Donnellan, T. L. Evans, M. L. Geai, M. T. Glasscoe, D. Green, D. R. Gurung, R. Heijenk, A. Hilborn, K. Hudnut, C. Huyck, W. W. Immerzeel, J. Liming, R. Jibson, A. Kääb, N. R. Khanal, D. Kirschbaum, P. D. A. Kraaijenbrink, D. Lamsal, L. Shiyin, L. Mingyang, D. McKinney, N. K. Nahirnick, N. Zhuotong, S. Ojha, J. Olsenholler, T. H. Painter, M. Pleasants, K. C. Pratima, Q. I. Yuan, B. H. Raup, D. Regmi, D. R. Rounce, A. Sakai, S. Donghui, J. M. Shea, A. B. Shrestha, A. Shukla, D. Stumm, M. van der Kooij, K. Voss, W. Xin, B. Weihs, D. Wolfe, W. Lizong, Y. Xiaojun, M. R. Yoder, N. Young, Geomorphic and geologic controls of geohazards induced by Nepal's 2015 Gorkha earthquake. *Science*. **351**, 140 (2016).

2. S. Allen, S. Cox, I. Owens, Rock avalanches and other landslides in the central Southern Alps of New Zealand: a regional study considering possible climate change impacts. *Landslides*. **8**, 33–48 (2011).

3. L. Fischer, R. S. Purves, C. Huggel, J. Noetzli, W. Haeberli, On the influence of topographic, geological and cryospheric factors on rock avalanches and rockfalls in high-mountain areas. *Natural Hazards and Earth System Sciences*. **12**, 241–254 (2012).

4. S. Gruber, R. Fleiner, E. Guegan, P. Panday, M.-O. Schmid, D. Stumm, P. Wester, Y. Zhang, L. Zhao, Review article: Inferring permafrost and permafrost thaw in the mountains of the Hindu Kush Himalaya region. *The Cryosphere*. **11**, 81–99 (2017).

5. A. Kääb, S. Leinss, A. Gilbert, Y. Bühler, S. Gascoin, S. G. Evans, P. Bartelt, E. Berthier, F. Brun, W.-A. Chao, D. Farinotti, F. Gimbert, W. Guo, C. Huggel, J. S. Kargel, G. J. Leonard, L. Tian, D. Treichler, T. Yao, Massive collapse of two glaciers in western Tibet in 2016 after surge-like instability. *Nature Geoscience*. **11**, 114–120 (2018).

6. M. Jacquemart, M. Loso, M. Leopold, E. Welty, E. Berthier, J. S. S. Hansen, J. Sykes, K. Tiampo, What drives large-scale glacier detachments? Insights from Flat Creek glacier, St. Elias Mountains, Alaska. *Geology*. **48**, 703–707 (2020).

7. S. G. Evans, K. B. Delaney, N. M. Rana, in *Snow and Ice-Related Hazards, Risks, and Disasters (Second Edition)*, W. Haeberli, C. Whiteman, Eds. (Elsevier, 2021; https://www.sciencedirect.com/science/article/pii/B9780128171295000044), pp. 541–596.

8. D. Kirschbaum, C. S. Watson, D. R. Rounce, D. H. Shugar, J. S. Kargel, U. K. Haritashya, P. Amatya, D. E. Shean, E. R. Anderson, M. Jo, The state of remote sensing capabilities of cascading hazards over High Mountain Asia. *Frontiers in Earth Science*. **7** (2019), doi:10.3389/feart.2019.00197.

9. D. Schneider, C. Huggel, W. Haeberli, R. Kaitna, Unraveling driving factors for large rock-ice avalanche mobility. *Earth Surface Processes and Landforms*. **36**, 1948–1966 (2011).

10. A. Kääb, M. Jacquemart, A. Gilbert, S. Leinss, L. Girod, C. Huggel, D. Falaschi, F. Ugalde, D. Petrakov, S. Chernomorets, M. Dokukin, F. Paul, S. Gascoin, E. Berthier, J. Kargel, Sudden large-volume detachments of low-angle mountain glaciers - more frequent than thought. *The Cryosphere*. **15**, 1751–1785 (2021).

11. S. G. Evans, N. F. Bishop, L. Fidel Smoll, P. Valderrama Murillo, K. B. Delaney, A. Oliver-Smith, A re-examination of the mechanism and human impact of catastrophic mass flows originating on Nevado Huascarán, Cordillera Blanca, Peru in 1962 and 1970. *Engineering Geology*. **108**, 96–118 (2009).

12. K. Upadhyay, A year later, no lessons learnt. *The Hindu* (2014), (available at https://www.thehindu.com/opinion/op-ed/a-year-later-no-lessons-learnt/article6120397.ece).

13. S. K. Allen, P. Rastner, M. Arora, C. Huggel, M. Stoffel, Lake outburst and debris flow disaster at Kedarnath, June 2013: hydrometeorological triggering and topographic predisposition. *Landslides*. **13**, 1479–1491 (2016).

14. R. Bhambri, M. Mehta, D. P. Dobhal, A. K. Gupta, B. Pratap, K. Kesarwani, A. Verma, Devastation in the Kedarnath (Mandakini) Valley, Garhwal Himalaya, during 16–17 June 2013: a remote sensing and ground-based assessment. *Natural Hazards*. **80**, 1801–1822 (2016).

15. PIB, Statement in Parliament by Union Home Minister Shri Amit Shah regarding avalanche in the upper catchment of Rishiganga River in Chamoli District of Uttarakhand. *Press Information Bureau (PIB)* (2021), (available at https://pib.gov.in/PressReleaseIframePage.aspx?PRID=1696552).

16. R. Hock, G. Rasul, C. Adler, S. Caceres, S. Gruber, Y. Hirabayashi, M. Jackson, A. Kääb, S. Kang, S. Kutuzov, A. Milner, U. Molau, S. Morin, B. Orlove, H. Steltzer, "Chapter 2: High Mountain Areas — Special Report on the Ocean and Cryosphere in a Changing Climate," *IPCC Special Report on the Ocean and Cryosphere in a Changing Climate* (2019), (available at https://www.ipcc.ch/srocc/chapter/chapter-2/).

17. K. S. Valdiya, Damming rivers in the tectonically resurgent Uttarakhand Himalaya. *Current Science*. **106**, 1658–1668 (2014).

18. R. A. Vaidya, D. J. Molden, A. B. Shrestha, N. Wagle, C. Tortajada, The role of hydropower in South Asia's energy future. *International Journal of Water Resources Development*. **37**, 367–391 (2021).

19. A. Diduck, J. Sinclair, D. Pratap, G. Hostetler, Achieving meaningful public participation in the environmental assessment of hydro development: case studies from Chamoli District, Uttarakhand, India. *Impact Assessment and Project Appraisal*. **25**, 219–231 (2007).

20. Kundan Singh v State of Uttarakhand, *High Court of Uttarakhand, India* (2019), vol. Writ Petition (P.I.L) No. 48 of 2019.

21. A. Shrestha, J. Steiner, S. Nepal, S. B. Maharjan, M. Jackson, G. Rasul, B. Bajracharya, Understanding the Chamoli flood: Cause, process, impacts, and context of rapid infrastructure development, (available at https://www.icimod.org/article/understanding-the-chamoli-flood-cause-process-impacts-and-context-of-rapid-infrastructure-development/).

22. Materials and methods are available as supplementary materials on Science Online.

23. W. Haeberli, C. Huggel, A. Kääb, S. Zgraggen-Oswald, A. Polkvoj, I. Galushkin, I. Zotikov, N. Osokin, The Kolka-Karmadon rock/ice slide of 20 September 2002: an extraordinary event of historical dimensions in North Ossetia, Russian Caucasus. *Journal of Glaciology*. **50**, 533–546 (2004).

24. F. Walter, F. Amann, A. Kos, R. Kenner, M. Phillips, A. de Preux, M. Huss, C. Tognacca, J. Clinton, T. Diehl, Y. Bonanomi, Direct observations of a three million cubic meter rock-slope collapse with almost immediate initiation of ensuing debris flows. *Geomorphology*. **351**, 106933 (2020).

25. J. Koshy, Scientists studying samples to know roots of Uttarakhand glacier disaster. *The Hindu* (2021), (available at https://www.thehindu.com/sci-tech/science/scientists-studying-samples-to-know-roots-of-uttarakhand-glacier-disaster/article33851727.ece).

26. R. G. McConnell, R. W. Brock, "Report on the Great Landslide at Frank, Alta. 1903," *Annual Report, Part VIII* (Department of the Interior Dominion of Canada, Ottawa, 1904), p. 17.

27. J. F. Orwin, J. J. Clague, R. F. Gerath, The Cheam rock avalanche, Fraser Valley, British Columbia, Canada. *Landslides*. **1**, 289–298 (2004).

28. A. Mitchell, S. McDougall, J. Aaron, M.-A. Brideau, Rock avalanche-generated sediment mass flows: definitions and hazard. *Front. Earth Sci.* **8**, 543937 (2020).

29. S. A. Dunning, The grain-size distribution of rock-avalanche deposits in valley confined settings. *Italian Journal of Engineering Geology and Environment*. **1**, 117–121 (2006).

30. D. H. Shugar, J. J. Clague, The sedimentology and geomorphology of rock avalanche deposits on glaciers. *Sedimentology*. **58**, 1762–1783 (2011).

31. M. Church, M. Jakob, What Is a Debris Flood? *Water Resources Research*. **56** (2020), doi:10.1029/2020WR027144.

32. Hindustan Times, Water supply back to normal, says Delhi Jal Board after Chamoli impact. *Hindustan Times* (2021), (available at https://www.hindustantimes.com/cities/others/normal-water-supply-to-resume-today-says-delhi-jal-board-101613412411000.html).

33. Uttarakhand Emergency Operations Centre, "Daily Report (A.T.R.:39)" (Dehradun, 2021).

34. S. Dutta, Fate of NTPC's Tapovan project hangs in balance after Rs 1,500 crore loss. *The Economic Times* (2021), (available at https://economictimes.indiatimes.com/industry/energy/power/fate-of-ntpcs-tapovan-project-hangs-in-balance-after-rs-1500-crore-loss/articleshow/80760066.cms).

35. J. Mazoomdaar, Behind hydel project washed away, a troubled trail to accident in 2011. *The Indian Express* (2021), (available at https://indianexpress.com/article/india/hydel-power-project-uttarakhand-flash-flood-glacier-burst-chamoli-district-7183561/).

36. R. F. Stuart-Smith, G. H. Roe, S. Li, M. R. Allen, Increased outburst flood hazard from Lake Palcacocha due to human-induced glacier retreat. *Nature Geoscience*. **14**, 85–90 (2021).

37. G. H. Roe, J. E. Christian, B. Marzeion, On the attribution of industrial-era glacier mass loss to anthropogenic climate change. *The Cryosphere*. **15**, 1889–1905 (2021).

38. W. Cramer, M. Auffhammer, C. Huggel, U. Molau, M. A. F. S. Dias, A. Solow, D. A. Stone, L. Tibig, in *Climate Change 2014: Impacts, Adaptation, and Vulnerability. Part A: Global and Sectoral Aspects. Contribution of Working Group II to the Fifth Assessment Report of the Intergovernmental Panel on Climate Change*, C. B. Field, V. R. Barros, D. J. Dokken, K. J. Mach, M. D. Mastrandrea, T. E. Bilir, M. Chatterjee, K. L. Ebi, Y. O. Estrada, R. C. Genova, B. Girma, E. S. Kissel, A. N. Levy, S. MacCracken, P. R. Mastrandrea, L. L. White, Eds. (Cambridge University Press, Cambridge, UK, 2014), pp. 979–1337.

39. E. K. Bessette-Kirton, J. A. Coe, A 36-year record of rock avalanches in the Saint Elias Mountains of Alaska, with implications for future hazards. *Frontiers in Earth Science*. **8**, 293 (2020).

40. J. Knight, S. Harrison, The impacts of climate change on terrestrial Earth surface systems. *Nature Climate Change*. **3**, 24–29 (2013).

41. N. Pepin, R. S. Bradley, H. F. Diaz, M. Baraer, E. B. Caceres, N. Forsythe, H. Fowler, G. Greenwood, M. Z. Hashmi, X. D. Liu, J. R. Miller, L. Ning, A. Ohmura, E. Palazzi, I. Rangwala, W. Schöner, I. Severskiy, M. Shahgedanova, M. B. Wang, S. N. Williamson, D. Q. Yang, Mountain Research Initiative EDW Working Group, Elevation-dependent warming in mountain regions of the world. *Nature Climate Change*. **5**, 424–430 (2015).

42. T. P. Sabin, R. Krishnan, R. Vellore, P. Priya, H. P. Borgaonkar, B. B. Singh, A. Sagar, in *Assessment of Climate Change over the Indian Region: A Report of the Ministry of Earth Sciences (MoES), Government of India*, R. Krishnan, J. Sanjay, C. Gnanaseelan, M. Mujumdar, A. Kulkarni, S. Chakraborty, Eds. (Springer, Singapore, 2020; https://doi.org/10.1007/978-981-15-4327-2_11), pp. 207–222.

43. M. F. Azam, P. Wagnon, E. Berthier, C. Vincent, K. Fujita, J. S. Kargel, Review of the status and mass changes of Himalayan-Karakoram glaciers. *Journal of Glaciology*. **64**, 61–74 (2018).

44. J. M. Maurer, J. M. Schaefer, S. Rupper, A. Corley, Acceleration of ice loss across the Himalayas over the past 40 years. *Science Advances*. **5**, eaav7266 (2019).

45. D. E. Shean, S. Bhushan, P. Montesano, D. R. Rounce, A. Arendt, B. Osmanoglu, A systematic, regional assessment of High Mountain Asia glacier mass balance. *Front. Earth Sci.* **7** (2020), doi:10.3389/feart.2019.00363.

46. R. Hugonnet, R. McNabb, E. Berthier, B. Menounos, C. Nuth, L. Girod, D. Farinotti, M. Huss, I. Dussaillant, F. Brun, A. Kääb, Accelerated global glacier mass loss in the early twenty-first century. *Nature*. **592**, 726–731 (2021).

47. S. Gruber, Derivation and analysis of a high-resolution estimate of global permafrost zonation. *The Cryosphere*. **6**, 221–233 (2012).

48. S. K. Allen, J. Fiddes, A. Linsbauer, S. S. Randhawa, B. Saklani, N. Salzmann, Permafrost Studies in Kullu District, Himachal Pradesh. *Current Science*. **111**, 550 (2016).

49. J. Noetzli, S. Gruber, Transient thermal effects in Alpine permafrost. *The Cryosphere*. **3**, 85–99 (2009).

50. B. K. Biskaborn, S. L. Smith, J. Noetzli, H. Matthes, G. Vieira, D. A. Streletskiy, P. Schoeneich, V. E. Romanovsky, A. G. Lewkowicz, A. Abramov, M. Allard, J. Boike, W. L. Cable, H. H. Christiansen, R. Delaloye, B. Diekmann, D. Drozdov, B. Etzelmüller, G. Grosse, M. Guglielmin, T. Ingeman-Nielsen, K. Isaksen, M. Ishikawa, M. Johansson, H. Johannsson, A. Joo, D. Kaverin, A. Kholodov, P. Konstantinov, T. Kröger, C. Lambiel, J.-P. Lanckman, D. Luo, G. Malkova, I. Meiklejohn, N. Moskalenko, M. Oliva, M. Phillips, M. Ramos, A. B. K. Sannel, D. Sergeev, C. Seybold, P. Skryabin, A. Vasiliev, Q. Wu, K. Yoshikawa, M. Zheleznyak, H. Lantuit, Permafrost is warming at a global scale. *Nature Communications*. **10**, 264 (2019).

51. J. Noetzli, H. H. Christiansen, K. Isaksen, S. Smith, L. Zhao, D. A. Streletskiy, Permafrost thermal state. *Bulletin of the American Meteorological Society*. **101**, S34–S36 (2020).

52. S. Gruber, W. Haeberli, Permafrost in steep bedrock slopes and its temperature-related destabilization following climate change. *Journal of Geophysical Research - Earth Surface*. **112** (2007), doi:10.1029/2006JF000547.

53. N. P. Rao, R. Rekapalli, D. Srinagesh, V. M. Tiwari, N. Hovius, K. L. Cook, M. Dietze, Seismological rockslide warnings in the Himalaya. *Science*. **372**, 247–247 (2021).

54. I. Kelman, M. H. Glantz, in *Reducing Disaster: Early Warning Systems For Climate Change* (Springer Netherlands, Dordrecht, 2014; http://link.springer.com/10.1007/978-94-017-8598-3_5), pp. 89–108.

55. S. K. McBride, A. Bostrom, J. Sutton, R. M. de Groot, A. S. Baltay, B. Terbush, P. Bodin, M. Dixon, E. Holland, R. Arba, P. Laustsen, S. Liu, M. Vinci, Developing post-alert messaging for ShakeAlert, the earthquake early warning system for the West Coast of the United States of America. *International Journal of Disaster Risk Reduction*. **50**, 101713–101713 (2020).

56. W. Pollock, J. Wartman, Human vulnerability to landslides. *GeoHealth*. **4** (2020), doi:10.1029/2020GH000287.

57. Sentinel Hub, (available at https://www.sentinel-hub.com/).

58. PlanetLabs, Education and Research - Satellite Imagery Solutions. *Planet* (2021), (available at https://planet.com/markets/education-and-research/).

59. Maxar, Uttarakhand Flooding, (available at https://www.maxar.com/open-data/uttarakhand-flooding).

60. S. Bhushan, D. Shean, Chamoli Disaster Pre-event 2-m DEM Composite: September 2015 (Version 1.0) [Data set] (2021), (available at https://zenodo.org/record/4554647).

61. D. Shean, S. Bhushan, E. Berthier, C. Deschamps-Berger, S. Gascoin, F. Knuth, Chamoli Disaster Post-event 2-m DEM Composite (February 10-11, 2021) and Difference Map (v1.0) [Data set] (2021), (available at https://zenodo.org/record/4558692).

62. r.avaflow | The mass flow simulation tool, (available at https://www.avaflow.org/).

63. R. K. Maikhuri, U. Rana, K. S. Rao, S. Nautiyal, K. G. Saxena, Promoting ecotourism in the buffer zone areas of Nanda Devi Biosphere Reserve: An option to resolve people—policy conflict. *International Journal of Sustainable Development & World Ecology*. **7**, 333–342 (2000).

64. P. K. Mukherjee, A. K. Jain, S. Singhal, N. B. Singha, S. Singh, K. Kumud, P. Seth, R. C. Patel, U-Pb zircon ages and Sm-Nd isotopic characteristics of the Lesser and Great Himalayan sequences, Uttarakhand Himalaya, and their regional tectonic implications. *Gondwana Research*. **75**, 282–297 (2019).

65. C. Montemagni, C. Montomoli, S. Iaccarino, R. Carosi, A. K. Jain, H.-J. Massonne, I. M. Villa, Dating protracted fault activities: microstructures, microchemistry and geochronology of the Vaikrita Thrust, Main Central Thrust zone, Garhwal Himalaya, NW India. *Geological Society, London, Special Publications*. **481**, 127–146 (2019).

66. K. S. Valdiya, O. P. Goel, Lithological subdivision and petrology of the Great Himalayan Vaikrita Group in Kumaun, India. *Proc. Indian Acad. Sci. (Earth Planet Sci.)*. **92**, 141–163 (1983).

67. N. I. Norrish, D. C. Wyllie, in *Landslides: Investigation and Mitigation* (Transportation Research Board Special Report, 1996; https://trid.trb.org/view/462513), pp. 391–425.

68. T. K. Raghuvanshi, Plane failure in rock slopes – A review on stability analysis techniques. *Journal of King Saud University - Science*. **31**, 101–109 (2019).

69. R. C. Patel, V. Adlakha, P. Singh, Y. Kumar, N. Lal, Geology, structural and exhumation history of the Higher Himalayan Crystallines in Kumaon Himalaya, India. *Journal of the Geological Society of India*. **77**, 47–72 (2011).

70. J. Célérier, T. M. Harrison, A. A. G. Webb, A. Yin, The Kumaun and Garwhal Lesser Himalaya, India: Part 1. structure and stratigraphy. *GSA Bulletin*. **121**, 1262–1280 (2009).

71. W. Xu, R. Bürgmann, Z. Li, An improved geodetic source model for the 1999 Mw 6.3 Chamoli earthquake, India. *Geophysical Journal International*. **205**, 236–242 (2016).

72. S. G. Evans, G. Scarascia-Mugnozza, A. L. Strom, R. L. Hermanns, A. Ischuk, S. Vinnichenko, in *Landslides from Massive Rock Slope Failure; NATO Science Series: IV, Earth and Environmental Sciences*, S. G. Evans, G. Scarascia-Mugnozza, A. L. Strom, R. L. Hermanns, Eds. (Springer, Dordrecht, 2006), pp. 3–52.

73. J. Fiddes, S. Gruber, TopoSCALE v.1.0: downscaling gridded climate data in complex terrain. *Geoscientific Model Development*. **7**, 387–405 (2014).

74. R. Bhambri, T. Bolch, R. K. Chaujar, S. C. Kulshreshtha, Glacier changes in the Garhwal Himalaya, India, from 1968 to 2006 based on remote sensing. *Journal of Glaciology*. **57**, 543–556 (2011).

75. V. Kumar, T. Shukla, M. Mehta, D. P. Dobhal, M. P. Singh Bisht, S. Nautiyal, Glacier changes and associated climate drivers for the last three decades, Nanda Devi region, Central Himalaya, India. *Quaternary International*. **575–576**, 213–226 (2021).

76. A. Banerjee, A. P. Dimri, K. Kumar, Temperature over the Himalayan foothill state of Uttarakhand: Present and future. *Journal of Earth System Science*. **130**, 33 (2021).

77. F. Brun, E. Berthier, P. Wagnon, A. Kaab, D. Treichler, A spatially resolved estimate of High Mountain Asia glacier mass balances from 2000 to 2016. *Nature Geoscience*. **10**, 668–673 (20117).

78. J. Obu, S. Westermann, A. Bartsch, N. Berdnikov, H. H. Christiansen, A. Dashtseren, R. Delaloye, B. Elberling, B. Etzelmüller, A. Kholodov, A. Khomutov, A. Kääb, M. O. Leibman, A. G. Lewkowicz, S. K. Panda, V. Romanovsky, R. G. Way, A. Westergaard-Nielsen, T. Wu, J. Yamkhin, D. Zou, Northern Hemisphere permafrost map based on TTOP modelling for 2000–2016 at 1 km2 scale. *Earth-Science Reviews*. **193**, 299–316 (2019).

79. NTPC Limited, NTPC works on modalities for release of compensation; Rescue operation continues in full swing. *NTPC Limited* (2021), (available at https://www.ntpc.co.in/en/media/press-releases/details/ntpc-works-modalities-release-compensation-rescue-operation-continues-full-swing).

80. N. Santoshi, Uttarakhand disaster: Reni gets 1st warning system in case of sudden water surge. *Hindustan Times* (2021), (available at https://www.hindustantimes.com/india-news/uttarakhand-disaster-reni-gets-1st-warning-system-in-case-of-sudden-water-surge-101613557801245.html#:~:text=Reni%2C the most-affected village,the village to recover bodies).

81. W. Schwanghart, R. Worni, C. Huggel, M. Stoffel, O. Korup, Uncertainty in the Himalayan energy–water nexus: estimating regional exposure to glacial lake outburst floods. *Environmental Research Letters*. **11**, 074005 (2016).

82. W. Schwanghart, M. Ryan, O. Korup, Topographic and seismic constraints on the vulnerability of Himalayan hydropower. *Geophysical Research Letters*. **45**, 8985–8992 (2018).

83. H. Regan, S. Gupta, Famous for its tree huggers, village at center of India glacier collapse warned of impending disaster for decades. No one listened. *CNN* (2021), (available at https://edition.cnn.com/2021/02/12/asia/india-glacier-raini-village-chipko-intl-hnk/index.html).

84. R. Guha, *The unquiet woods: ecological change and peasant resistance in the Himalaya* (Oxford University Press, New Delhi, 1989).

85. S. Pathak, *The Chipko Movement: A People's History* (Permanent Black, New Delhi, 2021).

86. R. J. Wasson, N. Juyal, M. Jaiswal, M. McCulloch, M. M. Sarin, V. Jain, P. Srivastava, A. K. Singhvi, The mountain-lowland debate: Deforestation and sediment transport in the upper Ganga catchment. *Journal of Environmental Management*. **88**, 53–61 (2008).

87. M. Mashal, H. Kumar, Before Himalayan Flood, India Ignored Warnings of Development Risks. *The New York Times* (2021), (available at https://www.nytimes.com/2021/02/08/world/asia/india-flood-ignored-warnings.html).

88. K. Upadhyay, Dams and damages. *The Hindu* (2021), (available at https://www.thehindu.com/opinion/op-ed/dams-and-damages/article33795426.ece).

89. Expert Body Report, "Assessment of Environmental Degradation and Impact of Hydroelectric projects during the June 2013 Disaster in Uttarakhand." (New Delhi, 2014), (available at http://gbpihedenvis.nic.in/PDFs/Disaster Data/Reports/Assessment_of_Environmental_Degradation.pdf).

90. M. P. S. Bisht, P. Rautela, Disaster looms large over Joshimath. *Current Science*. **98**, 1271–1271 (2010).

91. Standing Committee on Energy, "43rd Report" (New Delhi, 2019), (available at http://164.100.47.193/lsscommittee/Energy/16_Energy_43.pdf).

92. SANDRP, Tapovan Vishnugad HPP: delays, damages and destructions. *South Asia Network on Dams, Rivers and People (SANDRP)* (2021), (available at https://sandrp.in/2021/02/20/tapovan-vishnugad-hpp-delays-damages-and-destructions/).

93. J. Grönwall, "Large dams and human rights obligations: The case of the Pancheshwar Multipurpose Project on the border between India and Nepal" (9789188495181,

748 Stockholm, 2020), (available at https://www.siwi.org/wp-
749 content/uploads/2020/07/Report_ICWC_HRBA_2020_WEB.pdf).

750 94. K. D. Morell, M. Sandiford, C. P. Rajendran, K. Rajendran, A. Alimanovic, D. Fink, J.
751 Sanwal, Geomorphology reveals active décollement geometry in the central Himalayan
752 seismic gap. *Lithosphere*. **7**, 247–256 (2015).

753 95. R. E. S. Moss, E. M. Thompson, D. Scott Kieffer, B. Tiwari, Y. M. A. Hashash, I.
754 Acharya, B. R. Adhikari, D. Asimaki, K. B. Clahan, B. D. Collins, S. Dahal, R. W.
755 Jibson, D. Khadka, A. Macdonald, C. L. M. Madugo, H. Benjamin Mason, M. Pehlivan,
756 D. Rayamajhi, S. Uprety, Geotechnical effects of the 2015 Magnitude 7.8 Gorkha,
757 Nepal, earthquake and aftershocks. *Seismological Research Letters*. **86**, 1514–1523
758 (2015).

759 96. S. P. Sati, S. Sharma, N. Rana, H. Dobhal, N. Juyal, Environmental implications of
760 Pancheshwar dam in Uttarakhand (Central Himalaya), India. *Current Science*. **116**,
761 1483–1489 (2019).

762 97. Alaknanda Hydro Power Co. Ltd. v Anuj Joshi & Others, *Supreme Court of India. Civil*
763 *Appeal No. 6736 of 2013.* (2013).

764 98. Alaknanda Hydro Power Co. Ltd. v Anuj Joshi & Others, *Supreme Court of India. Reply*
765 *Affidavit on Behalf of Respondent/State of Uttarakhand to I.A. No. 28979 of 2020* (2020).

766 99. D. Mishra, Power Ministry Wanted to Dilute Rules So Hydro Projects Can Release Even
767 Less Water. *The Wire* (2021), (available at https://thewire.in/government/power-
768 ministry-dilute-environemntal-flow-rules-so-hydro-projects).

769 100. M. J. Froude, D. N. Petley, Global fatal landslide occurrence from 2004 to 2016. *Natural*
770 *Hazards and Earth System Sciences*. **18**, 2161–2181 (2018).

771 101. A. Stäubli, S. U. Nussbaumer, S. K. Allen, C. Huggel, M. Arguello, F. Costa, C.
772 Hergarten, R. Martínez, J. Soto, R. Vargas, E. Zambrano, M. Zimmermann, in *Climate*
773 *Change, Extreme Events and Disaster Risk Reduction: Towards Sustainable*
774 *Development Goals*, S. Mal, R. B. Singh, C. Huggel, Eds. (Springer International
775 Publishing, Cham, 2018; https://doi.org/10.1007/978-3-319-56469-2_2), *Sustainable*
776 *Development Goals Series*, pp. 17–41.

777 102. A. Pralong, M. Funk, On the instability of avalanching glaciers. *Journal of Glaciology*.
778 **52**, 31–48 (2006).

779 103. M. Van Wyk de Vries, *MaxVWDV/glacier-image-velocimetry: Glacier Image*
780 *Velocimetry (GIV)* (2021;
781 https://zenodo.org/record/4548848/preview/MaxVWDV/glacier-image-velocimetry-
782 v0.8.0.zip).

104. M. Van Wyk de Vries, A. D. Wickert, Glacier Image Velocimetry: an open-source toolbox for easy and rapid calculation of high-resolution glacier velocity fields. *The Cryosphere*, 1–31 (2021).

105. S. van der Walt, J. L. Schönberger, J. Nunez-Iglesias, F. Boulogne, J. D. Warner, N. Yager, E. Gouillart, T. Yu, scikit-image: image processing in Python. *PeerJ*. **2**, e453 (2014).

106. D. E. Shean, O. Alexandrov, Z. M. Moratto, B. E. Smith, I. R. Joughin, C. Porter, P. Morin, An automated, open-source pipeline for mass production of digital elevation models (DEMs) from very-high-resolution commercial stereo satellite imagery. *ISPRS Journal of Photogrammetry and Remote Sensing*. **116**, 101–117 (2016).

107. R. A. Beyer, O. Alexandrov, S. McMichael, The Ames Stereo Pipeline: NASA's open source software for deriving and processing terrain data. *Earth and Space Science*. **5**, 537–548 (2018).

108. P. Lacroix, Landslides triggered by the Gorkha earthquake in the Langtang valley, volumes and initiation processes. *Earth, Planets and Space*. **68** (2016), doi:10.1186/s40623-016-0423-3.

109. R. Hoste-Colomer, L. Bollinger, H. Lyon-Caen, L. B. Adhikari, C. Baillard, A. Benoit, M. Bhattarai, R. M. Gupta, E. Jacques, T. Kandel, B. P. Koirala, J. Letort, K. Maharjan, R. Matrau, R. Pandey, C. Timsina, Lateral variations of the midcrustal seismicity in western Nepal: Seismotectonic implications. *Earth and Planetary Science Letters*. **504**, 115–125 (2018).

110. F. Dammeier, J. R. Moore, F. Haslinger, S. Loew, Characterization of alpine rockslides using statistical analysis of seismic signals. *Journal of Geophysical Research: Earth Surface*. **116**, F04024 (2011).

111. F. Fuchs, W. Lenhardt, G. Bokelmann, the AlpArray Working Group, Seismic detection of rockslides at regional scale: examples from the Eastern Alps and feasibility of kurtosis-based event location. *Earth Surface Dynamics*. **6**, 955–970 (2018).

112. J. Deparis, D. Jongmans, F. Cotton, L. Baillet, F. Thouvenot, D. Hantz, Analysis of rock-fall and rock-fall avalanche seismograms in the French Alps. *Bulletin of the Seismological Society of America*. **98**, 1781–1796 (2008).

113. C. Hibert, A. Mangeney, G. Grandjean, N. M. Shapiro, Slope instabilities in Dolomieu crater, Réunion Island: From seismic signals to rockfall characteristics. *Journal of Geophysical Research: Earth Surface*. **116**, F04032 (2011).

114. G. Le Roy, A. Helmstetter, D. Amitrano, F. Guyoton, R. L. Roux-Mallouf, Seismic analysis of the detachment and impact phases of a rockfall and application for estimating rockfall volume and free-fall height. *Journal of Geophysical Research: Earth Surface*. **124**, 2602–2622 (2019).

115. A. Burtin, L. Bollinger, R. Cattin, J. Vergne, J. L. Nábělek, Spatiotemporal sequence of Himalayan debris flow from analysis of high-frequency seismic noise. *Journal of Geophysical Research: Earth Surface*. **114** (2009), doi:https://doi.org/10.1029/2008JF001198.

116. G. Monsalve, A. Sheehan, V. Schulte-Pelkum, S. Rajaure, M. R. Pandey, F. Wu, Seismicity and one-dimensional velocity structure of the Himalayan collision zone: Earthquakes in the crust and upper mantle. *Journal of Geophysical Research: Solid Earth*. **111** (2006), doi:https://doi.org/10.1029/2005JB004062.

117. Z. Zhang, S. Klemperer, Crustal structure of the Tethyan Himalaya, southern Tibet: new constraints from old wide-angle seismic data. *Geophysical Journal International*. **181**, 1247–1260 (2010).

118. D. Farinotti, M. Huss, J. J. Fürst, J. Landmann, H. Machguth, F. Maussion, A. Pandit, A consensus estimate for the ice thickness distribution of all glaciers on Earth. *Nature Geoscience*. **12**, 168–173 (2019).

119. T. H. Assumpção, I. Popescu, A. Jonoski, D. P. Solomatine, Citizen observations contributing to flood modelling: opportunities and challenges. *Hydrology and Earth System Sciences*. **22**, 1473–1489 (2018).

120. M. Mergili, J.-T. Fischer, J. Krenn, S. P. Pudasaini, r.avaflow v1, an advanced open-source computational framework for the propagation and interaction of two-phase mass flows. *Geoscientific Model Development*. **10**, 553–569 (2017).

121. M. Mergili, S. P. Pudasaini, *r.avaflow - The mass flow simulation tool* (2020; https://www.avaflow.org/).

122. S. P. Pudasaini, M. Mergili, A multi-phase mass flow model. *Journal of Geophysical Research: Earth Surface*. **124**, 2920–2942 (2019).

123. S. Gascoin, M. Grizonnet, M. Bouchet, G. Salgues, O. Hagolle, Theia Snow collection: high-resolution operational snow cover maps from Sentinel-2 and Landsat-8 data. *Earth System Science Data*. **11**, 493–514 (2019).

124. Uttarakhand DMMC, "List of Missing Persons" (Uttarakhand Disaster Mitigation and Management Centre (DMMC), Dehradun, 2021).

Acknowledgements: We acknowledge all the individuals who shared videos, images, and other 'on-the-ground' observations in real-time and soon after the event. These eyewitness accounts greatly aided our interpretations. This study was coordinated with the IACS and IPA Standing Group on Glacier and Permafrost Hazards in Mountains (http://www.gaphaz.org). PlanetLabs, Maxar, and CNES provided prioritized satellite tasking and rapid data access and for that, we are grateful. We thank the NGA EnhancedView Program Management Office for supporting Level-1B image access under the NextView License and composite DEM release. Any use of trade, firm, or product names is for descriptive purposes only does not imply

endorsement by the U.S. Government. The views and interpretations in this publication are those of the authors and are not necessarily attributable to their organizations. We thank three anonymous reviewers for their insightful comments, which strengthened this paper. Finally, this paper is dedicated to those who lost their lives in the Chamoli disaster, and those who remain missing.

Funding:

- Alexander von Humboldt Foundation, Government of the Federal Republic of Germany (AM)
- Centre National d'Études Spatiales internal funding (EB)
- Centre National d'Études Spatiales, Programme National de Télédétection Spatiale PNTS-2018-4 (SG)
- CIRES Graduate Research Fellowship (MJ)
- Department of Science and Technology, Government of India (AKumar, KS)
- European Space Agency CCI programme and EarthExplorer10 4000123681/18/I-NB, 4000109873/14/I-NB, 4000127593/19/I-NS, 4000127656/19/NL/FF/gp (AKääb)
- European Space Agency Glaciers CCI+ 4000127593/19/I-NB (FP)
- Future Investigators in NASA Earth and Space Science and Technology 80NSSC19K1338 (SB)
- ICIMOD core funds (JS)
- Natural Sciences and Engineering Research Council (NSERC) 04207-2020 (DHS)
- NASA Cryosphere 80NSSC20K1442 (UKH, JSK)
- NASA High Mountain Asia Team (HiMAT-1) 80NSSC19K0653 (UKH, JSK, DHS)
- NASA High Mountain Asia Team (HiMAT-2) 80NSSC20K1594 (SR)
- NASA High Mountain Asia Team (HiMAT-2) 80NSSC20K1595 (DES)
- NASA Interdisciplinary Research in Earth Science 80NSSC18K0432 (UKH, JSK)
- Roshydromet R&D Plan, Theme 6.3.2 AAAA-A20-120031990040-7 (MD)
- Swiss Agency for Development and Cooperation (SDC) 7F-08954.01.03 (SA, HF, CH)
- Swiss National Science Foundation 200020_179130 (JF)
- Swiss National Science Foundation, project "Process-based modelling of global glacier changes (PROGGRES)", Grant Nr. 200021_184634 (DF)
- Swiss Federal Excellence Postdoc Award (AS)

Author contributions: (main author list order preserved for each section): **(1) Writing – original draft:** DHS, MJ, DS, SB, KU, SM, MVWdV, MMergili, AE, EB, JLC, JJC, SAD, HF, SG, UKH, CH, AKääb, JSK, JLK, PL, DP, SR, ME, DF, JN; (2) **Writing – review & editing:** all authors; **(3) Methodology, Investigation, Formal analysis –** satellite-based geomorphological mapping: DHS, WS, JLC, JJC, MD, SAD, UKH, CH, AKääb, SJC, FP, MJW; flow modeling: AS, MM, UKH; energy-balance modeling: AKääb, JSK, JLK; DEM production: DS, SB, CDB, EB, SG; climate, weather, and geology analysis: MJ, DS,

MMcDonnell, RB, SA, HF, UKH, JSK, SG, SR, APD, JF, MK, SL, SM, JN, UM, AM, IR, JS; social and economic impacts: KU, SM, SAD, JSK, MFA, ME; video analysis: AE, FP; precursory motion: MVWdV, SG, AKääb, MD; seismology: PL, MJ; field mapping: MFA, AKumar, IR, KS; **(4) Data curation –** DHS, DS, SB, WS, MVWdV, MMergili, CDB, MMcDonnell, EB, SG, JLK, PL, SR, MJ; **(5) Visualization –** DHS, MJ, DS, SB, WS, MVWdV, MM, AE, CDB, EB, SG, AKääb, JLK, PL, DF; **(6) Project administration –** DHS.

Competing interests: Authors declare that they have no competing interests.

Data availability: We used publicly available data sources whenever possible. The Sentinel-2 data are available from (*57*). PlanetScope satellite image data are available through Planet's Education and Research Program (*58*). Pre- and post-event very-high resolution satellite images are available through Maxar's Open Data Program (*59*), with others available via the NGA NextView License. Airbus/CNES (Pléiades) images were made publicly available through the International Charter: Space and Major Disasters. The derived DEM Composite data are available from (*60*, *61*). ERA5 data are available from the Copernicus climate Data Store.

Code availability: The r.avaflow model is available at (*62*). The r.avaflow code used for the simulation, the start script, and all of the input data are available at [insert link when available] along with a brief tutorial on how to reproduce the results presented in the paper.

Supplementary Materials

Supplementary Text
Materials and Methods
Figs. S1 to S17
Tables S1 to S5
References (62-124)